

Implementing fault-tolerant non-Clifford gates using the $[[8,3,2]]$ color code

Daniel Honciuc Menendez,¹ Annie Ray,^{2,3} and Michael Vasmer^{2,3}

¹*Department of Physics, University of Toronto, Toronto, ON M5S 1A7, Canada*

²*Institute for Quantum Computing, University of Waterloo, Waterloo, ON N2L 3G1, Canada*

³*Perimeter Institute for Theoretical Physics, Waterloo, ON N2L 2Y5, Canada*

(Dated: September 15, 2023)

Quantum computers promise to solve problems that are intractable for classical computers, but qubits are vulnerable to many sources of error, limiting the depth of the circuits that can be reliably executed on today’s quantum hardware. Quantum error correction has been proposed as a solution to this problem, whereby quantum information is protected by encoding it into a quantum error-correcting code. But protecting quantum information is not enough, we must also process the information using logic gates that are robust to faults that occur during their execution. One method for processing information fault-tolerantly is to use quantum error-correcting codes that have logical gates with a tensor product structure (transversal gates), making them naturally fault-tolerant. Here, we test the performance of a code with such transversal gates, the $[[8,3,2]]$ color code, using trapped-ion and superconducting hardware. We observe improved performance (compared to no encoding) for encoded circuits implementing non-Clifford gates, a class of gates that are essential for achieving universal quantum computing. In particular, we find improved performance for an encoded circuit implementing the control-control Z gate, a key gate in Shor’s algorithm. Our results illustrate the potential of using codes with transversal gates to implement non-trivial algorithms on near-term quantum hardware.

I. INTRODUCTION

Quantum error correction (QEC) promises to unlock the full potential of quantum computing, by protecting fragile qubits from the effects of decoherence [1–3]. But it is not enough to merely preserve the quantum information stored in a qubit register, we also need to perform a universal set of logical gates in a fault-tolerant manner [4]. Logical gates in the Clifford group (the unitaries that map Pauli operators to Pauli operators) are often relatively straightforward to implement fault-tolerantly in a given QEC code, however they are not universal. In fact, no QEC code can have a transversal and universal set of logical gates [5]. To obtain a universal gate set we need an additional non-Clifford gate [6], but implementing gates from this class fault-tolerantly is often difficult, usually requiring complex procedures such as magic state distillation [7, 8].

Certain QEC codes with special structure have transversal non-Clifford gates, where a transversal gate is a gate that acts as a tensor product unitaries that do not entangle different qubits in the same QEC code block. Examples of such gates include the transversal CNOT available in all CSS codes, and any gate acting as a tensor product of single-qubit unitaries. Transversal gates are naturally fault-tolerant as they do not spread errors within a code block.

There exists a family of codes known as triorthogonal codes [9] with transversal non-Clifford gates, implemented by tensor products of $T = \text{diag}(1, \exp(i\pi/4))$. Certain (generalized) triorthogonal codes have transversal entangling non-Clifford gates, the smallest of which (to our knowledge) is the $[[8,3,2]]$ color code [10, 11], which has a transversal $\text{CCZ} = \text{diag}(1, 1, 1, 1, 1, 1, 1, -1)$ gate. From a fault-tolerance perspective, it is particularly

desirable to implement complex entangling gates using single-qubit gates, as single-qubit gates are often an order of magnitude less noisy than entangling gates in many hardware platforms [12–17]. Using small codes to demonstrate fault-tolerant Clifford and non-Clifford operations has previously been suggested [18] and implemented in NMR [19, 20], trapped-ion [21–24], and superconducting hardware [25–27].

Here, we perform experiments on superconducting and trapped-ion hardware platforms to compare the performance of the encoded gates of the $[[8,3,2]]$ code with the same gates executed with no encoding. We find that the encoded gates perform better than their non-encoded counterparts in every case where the encoded gate is non-Clifford, even though the encoded circuits contain more entangling gates than the unencoded circuits. Notably, we observe improved performance for the CCZ gate, which is the dominant gate in circuits such as adders [28, 29] and the modular exponentiation used in Shor’s algorithm [30, 31].

The remainder of this article is structured as follows. In Section II, we review the definition of the $[[8,3,2]]$ code and its transversal logical gates. In Section III, we give fault-tolerant circuits for preparing encoded states of the $[[8,3,2]]$ code and for logical measurements. In Section IV, we describe our experiments on quantum hardware and their results, and we conclude with Section V.

II. THE $[[8,3,2]]$ COLOR CODE

The $[[8,3,2]]$ color code is a stabilizer code [32], encoding 3 logical qubits into 8 physical qubits with distance 2 (meaning that it can detect any single-qubit error). It is convenient to define the code using a geometric represen-

tation, where the physical qubits reside at the vertices of a cube, as shown in Fig. 1. The stabilizer group is generated by an X -type operator acting on all the qubits, and by Z -type operators associated with the faces of the cube. Concretely, using the qubit indices in Fig. 1, the stabilizer group is

$$\mathcal{S} = \langle X^{\otimes 8}, Z_0Z_1Z_2Z_3, Z_4Z_5Z_6Z_7, Z_0Z_1Z_4Z_5, Z_0Z_2Z_4Z_6 \rangle, \quad (1)$$

where Z_i denotes a Pauli Z operator acting on qubit i etc. We note that the stabilizer generators in Eq. (1) are either X -type or Z -type, meaning that the $[[8,3,2]]$ code is a CSS code [33, 34].

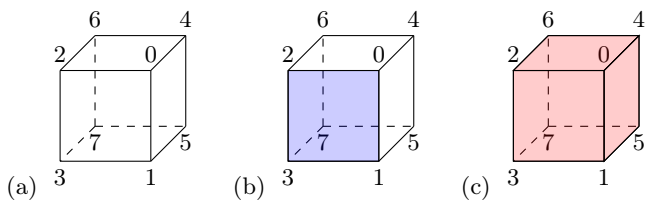


Figure 1. Geometric representation of the $[[8,3,2]]$ code. (a) The physical qubits reside at the vertices of the cube. (b) Z -type stabilizers are associated with faces, for example the blue face has an associated stabilizer $Z_0Z_1Z_2Z_3$. (c) The X -type stabilizer acts on all the qubits.

The logical operators of the $[[8,3,2]]$ code also have a geometric interpretation. Logical X operators are associated with the faces of the cube, and logical Z operators with the edges of the cube. We can choose the following basis of logical Pauli operators

$$\begin{aligned} \overline{X}_1 &= X_0X_1X_2X_3, & \overline{Z}_1 &= Z_0Z_4, \\ \overline{X}_2 &= X_0X_1X_4X_5, & \overline{Z}_2 &= Z_0Z_2, \\ \overline{X}_3 &= X_0X_2X_4X_6, & \overline{Z}_3 &= Z_0Z_1, \end{aligned} \quad (2)$$

where we use overlines to distinguish operators acting on the logical qubits from operators acting on the physical qubits.

The $[[8,3,2]]$ code is notable for having a non-Clifford transversal gate, CCZ implemented by T and T^\dagger gates. Specifically,

$$\overline{\text{CCZ}} = T_0T_1^\dagger T_2^\dagger T_3T_4^\dagger T_5T_6T_7^\dagger. \quad (3)$$

This gate again has a geometric interpretation: vertices and edges of the cube form a bipartite graph and CCZ is implemented by applying T to (the qubits on) one set of the vertices and T^\dagger to the other. The transversality of CCZ and Pauli X imply that the $[[8,3,2]]$ code also has transversal $\text{CZ} = \text{diag}(1, 1, 1, -1)$ gates, as follows

$$\begin{aligned} \overline{\text{CZ}}_{12} &= S_0S_2^\dagger S_4^\dagger S_6, \\ \overline{\text{CZ}}_{13} &= S_0S_1^\dagger S_4^\dagger S_5, \\ \overline{\text{CZ}}_{23} &= S_0S_1^\dagger S_2^\dagger S_3, \end{aligned} \quad (4)$$

where $S = T^2$ and CZ_{ij} acts on logical qubits i and j .

III. FAULT-TOLERANT CIRCUITS

For an error-detecting code such as the $[[8,3,2]]$ code, we say that a circuit is fault-tolerant if any single-qubit error on the input state or an error at any single location in the circuit can at worst lead to a detectable error on the output state. A circuit location can be a state preparation, gate, or measurement. We need only consider Pauli errors due to error discretization [35]. And we note that as the $[[8,3,2]]$ code is a CSS code, it is sufficient to analyse X and Z errors independently. We remark that the logical CCZ and CZ gates discussed in Section II are transversal and are therefore trivially fault-tolerant. We also need fault-tolerant circuits for logical measurement and logical state preparation, and we now discuss each of these in turn.

As the $[[8,3,2]]$ code is a CSS code, we can do a fault-tolerant measurement of the logical qubits in the X or Z basis by measuring all of the physical qubits in the X or Z basis, respectively, and processing the classical outcomes [35]. In the case of an error-detecting code such as the $[[8,3,2]]$ code, the classical processing is especially simple: we simply discard any measurement result that corresponds to a state that is not a $+1$ eigenvalue of the stabilizers. For example, when measuring in the X basis we accept any result whose parity is even, i.e., a $+1$ eigenstate of $X^{\otimes 8}$. This is fault-tolerant because single-qubit errors before the measurements are detectable by definition, and any single measurement error is equivalent to a single-qubit error before the measurement.

A. GHZ state preparation

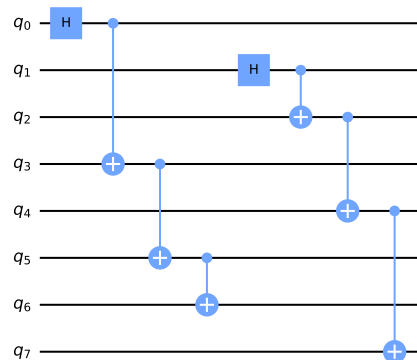


Figure 2. Fault-tolerant circuit for preparing the $|\text{GHZ}\rangle$ state in the $[[8,3,2]]$ code.

First we consider a fault-tolerant circuit for preparing the logical GHZ state, $|\text{GHZ}\rangle = (|000\rangle + |111\rangle)/\sqrt{2}$. Our circuit (shown in Fig. 2) factorizes into two independent and identical sub-circuits acting on qubits $0, 3, 6$ and qubits $1, 2, 4, 7$ (the two bipartite sets discussed in Section II). The $[[8,3,2]]$ code can detect any

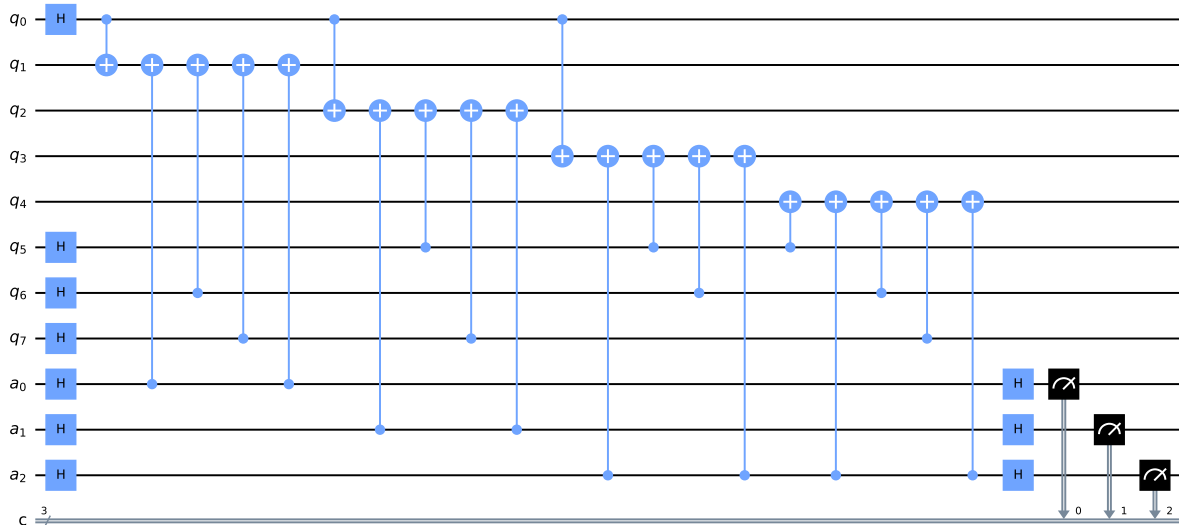


Figure 3. Fault-tolerant circuit for preparing the state $|+++ \rangle$ in the $[[8,3,2]]$ code. The qubits a_1 , a_2 and a_3 are flag qubits whose purpose is to detect certain Z errors that could cause logical errors. If we measure the three flag qubits to be in the $|0\rangle$ state then we accept the output.

weight ≤ 3 X error and so we only need to consider the four-qubit errors $X_0X_3X_5X_6$ and $X_1X_2X_4X_7$. However, each of these errors is in fact a logical $\bar{X}_1\bar{X}_2\bar{X}_3$ operator and so leaves the target $|\text{GHZ}\rangle$ state invariant. The only possible Z errors are weight one (detectable) and weight two (non-detectable). However, one can verify that all the non-detectable errors have trivial action on the target $|\text{GHZ}\rangle$ state. For example, the first CNOT could fail giving a Z_1Z_2 error, but this implements a logical $\bar{Z}_2\bar{Z}_3$ operator (see Eq. (2)) and hence leaves the target $|\text{GHZ}\rangle$ state invariant.

B. $|+++ \rangle$ state preparation

Next, we provide a fault-tolerant circuit for preparing the $|+++ \rangle$ state, shown in Fig. 3. In this circuit, the potentially problematic errors are those that can propagate through the CNOT gates. Consider, for example, the CNOT gates with qubit 0 as the control. The possible multi-qubit X errors that can arise from these gates are

$$\begin{aligned} X_0X_3 & \text{ (detectable),} \\ X_0X_2X_3 & \text{ (detectable),} \\ X_0X_1X_2X_3 & \text{ } (\bar{X}_1), \end{aligned} \quad (5)$$

where the only non-detectable error has trivial action on the target encoded state. The same is true for the other groups of CNOT gates with the same target. Certain Z errors can also propagate through CNOT gates. For example, consider the CNOT gates with qubit 1 as the target. The possible multi-qubit Z errors that can arise

from these gates are

$$\begin{aligned} Z_1Z_{a_0} & \text{ (detectable),} \\ Z_1Z_7Z_{a_0} & \text{ (detectable),} \\ Z_1Z_6Z_7 & \text{ (detectable),} \\ Z_1Z_6Z_7Z_{a_0} & \text{ (detectable),} \\ Z_0Z_1Z_6Z_7 & \text{ (stabilizer).} \end{aligned} \quad (6)$$

The purpose of the flag qubit [36], a_0 , is to make the error $Z_1Z_7 = \bar{Z}_1\bar{Z}_2$ detectable. Similarly, the flag qubits a_1 and a_2 catch the errors Z_2Z_7 , Z_3Z_6 and Z_4Z_6 .

IV. EXPERIMENTAL RESULTS

We investigate the performance of circuits comprised of three parts: state preparation, a transversal logical gate, and logical measurement.

For the state preparation part, we consider either $|\text{GHZ}\rangle$ or $|+++ \rangle$ state preparation, using the circuits described in Section III. For the logical gate part, we consider one of the 16 possible products of the transversal logical CCZ , CZ_{12} , CZ_{02} and CZ_{01} gates available in the $[[8,3,2]]$ code. For the logical measurement part, we consider transversal Z basis and X basis measurements. In the encoded case, the fault-tolerant measurement involves post-selection and we provide the post-selection rates for each of the experiments in Appendix B 2.

We test these circuits on two quantum computers: `ibmq_mumbai`, a 27-qubit device developed by IBM [37], and `ionq-11q`, an 11-qubit device developed by IonQ [13]. The IonQ device has all-to-all qubit connectivity, whereas

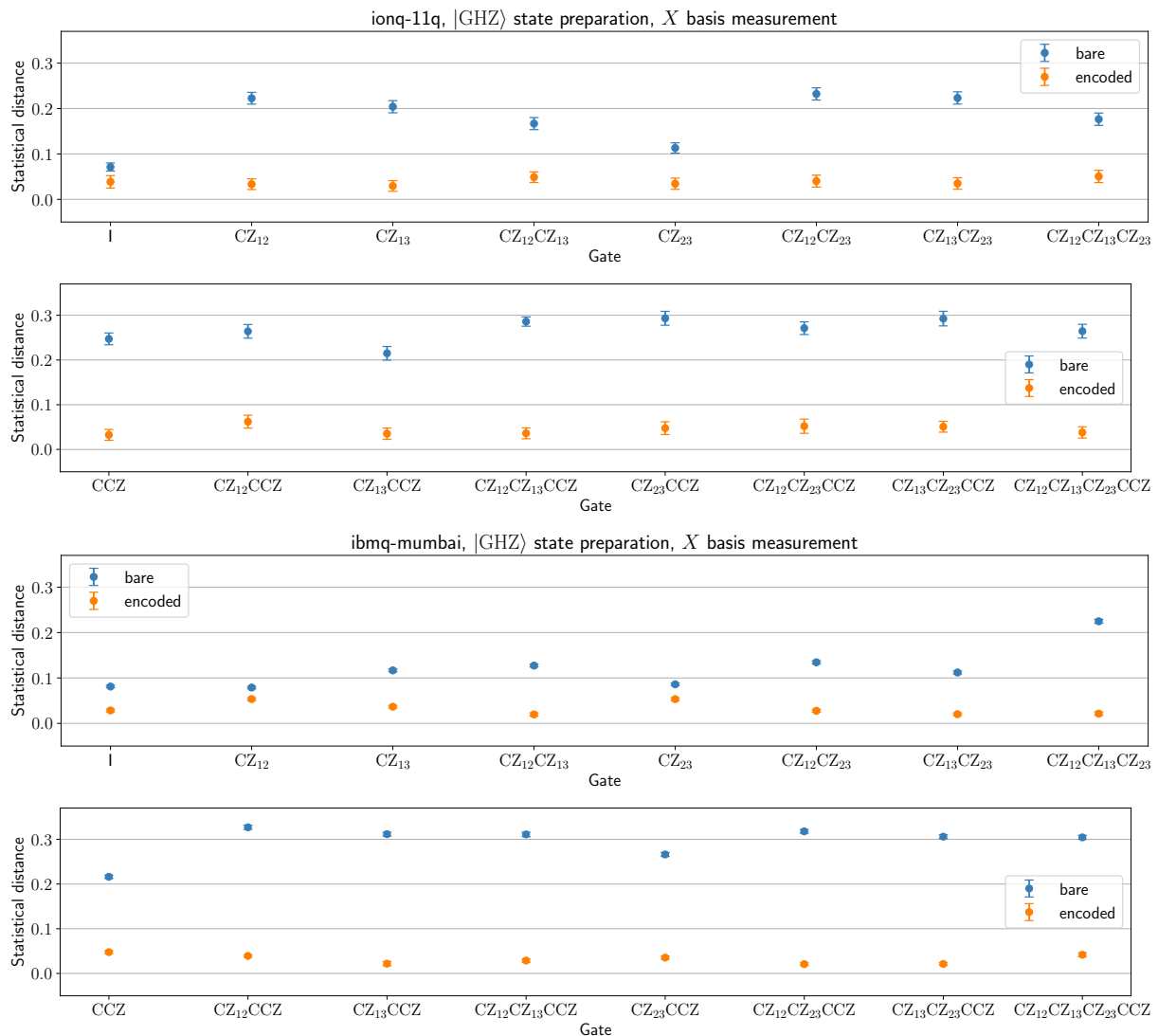


Figure 4. Performance of bare (unencoded) and encoded versions of circuits for preparing states of the form $g|\text{GHZ}\rangle$, where g is a transversal gate of the $[[8,3,2]]$ code. In each case, we measure the qubits in the X basis and we plot the statistical distance of the observed measurement distribution from the ideal distribution. The upper two plots show the data for `ionq-11q`, where we ran 1024 shots for each circuit, and the lower two plots show the data for `ibmq_mumbai` where we ran 10,000 shots for each circuit. In both cases, the error bars are calculated using bootstrap resampling.

the IBM device has “heavy-hexagon” qubit connectivity [38], see Appendix A. We only consider $|\text{GHZ}\rangle$ state preparation on the IBM device, as our circuit for preparing logical $|+++ \rangle$ states (Fig. 3) is only implementable on the IBM device with SWAP gates, and as a result is no longer fault-tolerant. We compare the performance of the encoded circuits against the performance of the bare (no encoding) circuits, using the statistical distance of the output distribution from the ideal output distribution as our metric.

We show the results for $|\text{GHZ}\rangle$ state preparation and X basis measurement in Fig. 4. For both devices and for every transversal gate, we observe improved performance of the encoded version of the circuit. The results

for Z basis measurement are qualitatively similar; see Appendix B 1.

We show the results for $|+++ \rangle$ state preparation and X basis measurement in Fig. 5. The bare version of the circuit performs better for transversal Clifford gates, whereas the encoded version performs better for transversal non-Clifford gates. Notably, we observe lower statistical distances for the preparation of the encoded magic state $\text{CCZ}|+++ \rangle$. We can attribute the difference between the results for Clifford and non-Clifford gates to the compilation of the three-qubit CCZ gate into a circuit involving multiple two-qubit gates on the IonQ device [39]. And the discrepancy between the results for $|+++ \rangle$ and $|\text{GHZ}\rangle$ state preparation is expected, given

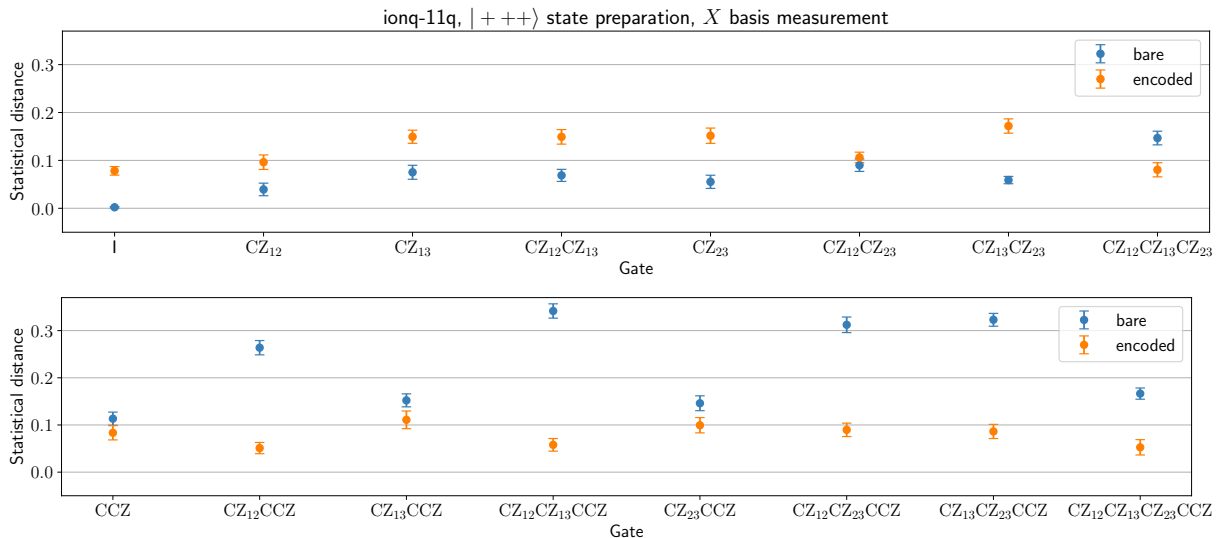


Figure 5. Performance of bare (unencoded) and encoded versions of circuits for preparing states of the form $g|+++ \rangle$, where g is a transversal gate of the $[[8,3,2]]$ code. In each case, we measure the qubits in the X basis and we plot the statistical distance of the observed measurement distribution from the ideal distribution. Each data point represents 1024 shots of the circuit performed on ionq-11q, and we use bootstrap resampling to calculate the error bars.

that the bare circuit for preparing the former requires only single-qubit gates and the latter requires two entangling gates. We again relegate the results for Z basis measurement to Appendix B 1, as they are qualitatively similar to the results for X basis measurement.

V. DISCUSSION

We have shown that using the $[[8,3,2]]$ code allows us to prepare certain (encoded) states more accurately (as measured by the statistical distance) than using the native gates to prepare the same (unencoded) states. We observe this advantage across a range of circuits on two different hardware platforms: IBM’s superconducting qubits and IonQ’s trapped-ion qubits. The all-to-all connectivity of the IonQ device that we used enabled us to run more circuits fault-tolerantly than we could on the IBM device. In particular, we were able to interrogate the performance of the $[[8,3,2]]$ code for preparing magic states of the form $g|+++ \rangle$, where $g \in CCZ \times \{I, CZ_{12}, CZ_{13}, CZ_{23}\}$. We observe an improved performance for the encoded version of circuits for preparing these states, illustrating the utility of codes like the $[[8,3,2]]$ code, where multi-qubit non-Clifford gates can be applied using single-qubit operations.

The $[[8,3,2]]$ is one example of a family of codes, known as generalized triorthogonal codes [40–42], with transversal multi-qubit Z rotations implemented by single-qubit gates. In future it would be interesting to test the performance of larger codes in this family with higher distance. For example, Ref. [42] gives a $[[64,6,4]]$ code with a transversal $CCZ^{\otimes 2}$ gate and it is possible that smaller

examples could be found using the techniques of [43–45].

As with any stabilizer code, the transversal gates of the $[[8,3,2]]$ code do not form a universal set of gates. Therefore, in order to use the $[[8,3,2]]$ code or a similar code to implement an actual quantum algorithm, we would need to supplement the transversal gates with additional fault-tolerant gates in order to obtain a universal gate set. One possibility worth considering would be to explore the implementation of logical gates via permutations of the physical qubits [46, 47], which can be fault-tolerant if implemented by qubit relabelling or physically moving the qubits.

ACKNOWLEDGEMENTS

Research at Perimeter Institute is supported in part by the Government of Canada through the Department of Innovation, Science and Economic Development Canada and by the Province of Ontario through the Ministry of Colleges and Universities. We acknowledge the support of the Natural Sciences and Engineering Research Council of Canada (NSERC). We thank IonQ for giving us access to their hardware through the IonQ Research Credits Program. We acknowledge CMC Microsystems for facilitating this research, specifically through their member access to the IBM Quantum Hub at PINQ². We thank Benjamin Brown, Joel Klassen and James Seddon for useful discussions. We thank Raymond Laflamme for comments on an earlier version of this manuscript.

Note added: We would like to bring the reader’s attention to a related work by Wang, Simsek and Criger [48], which appears in the same arXiv posting.

- [1] Peter W. Shor. “Scheme for reducing decoherence in quantum computer memory”. *Phys. Rev. A* **52**, R2493–R2496 (1995).
- [2] A. M. Steane. “Error correcting codes in quantum theory”. *Phys. Rev. Lett.* **77**, 793–797 (1996).
- [3] I. L. Chuang and R. Laflamme. “Quantum Error Correction by Coding” (1995). arxiv:quant-ph/9511003.
- [4] P.W. Shor. “Fault-tolerant quantum computation”. In *Proceedings of 37th Conference on Foundations of Computer Science*. Pages 56–65. (1996).
- [5] Bryan Eastin and Emanuel Knill. “Restrictions on Transversal Encoded Quantum Gate Sets”. *Phys. Rev. Lett.* **102**, 110502 (2009).
- [6] Gabriele Nebe, E. M. Rains, and N. J. A. Sloane. “The Invariants of the Clifford Groups”. *Designs, Codes and Cryptography* **24**, 99–122 (2001).
- [7] Sergey Bravyi and Alexei Kitaev. “Universal quantum computation with ideal Clifford gates and noisy ancillas”. *Phys. Rev. A* **71**, 022316 (2005).
- [8] E. Knill. “Fault-Tolerant Postselected Quantum Computation: Schemes” (2004). arxiv:quant-ph/0402171.
- [9] Sergey Bravyi and Jeongwan Haah. “Magic-state distillation with low overhead”. *Phys. Rev. A* **86**, 052329 (2012).
- [10] Aleksander Kubica, Beni Yoshida, and Fernando Pastawski. “Unfolding the color code”. *New J. Phys.* **17**, 083026 (2015).
- [11] Earl Campbell. “The smallest interesting colour code”. <https://earlrcampbell.com/2016/09/26/the-smallest-interesting-colour-code/> (2016).
- [12] C. J. Ballance, T. P. Harty, N. M. Linke, M. A. Sepiol, and D. M. Lucas. “High-fidelity quantum logic gates using trapped-ion hyperfine qubits”. *Phys. Rev. Lett.* **117**, 060504 (2016).
- [13] K. Wright, K. M. Beck, S. Debnath, J. M. Amini, Y. Nam, N. Grzesiak, J.-S. Chen, N. C. Pisenti, M. Chmielewski, C. Collins, K. M. Hudek, J. Mizrahi, J. D. Wong-Campos, S. Allen, J. Apisdorf, P. Solomon, M. Williams, A. M. Ducore, A. Blinov, S. M. Kreike-meier, V. Chaplin, M. Keesan, C. Monroe, and J. Kim. “Benchmarking an 11-qubit quantum computer”. *Nat. Commun.* **10**, 5464 (2019).
- [14] Petar Jurcevic, Ali Javadi-Abhari, Lev S Bishop, Isaac Lauer, Daniela F Bogorin, Markus Brink, Lauren Capel-luto, Oktay Günlük, Toshinari Itoko, Naoki Kanazawa, Abhinav Kandala, George A Keefe, Kevin Krsulich, William Landers, Eric P Lewandowski, Douglas T McClure, Giacomo Nannicini, Adinath Narasgond, Hasan M Nayfeh, Emily Pritchett, Mary Beth Rothwell, Srikanth Srinivasan, Neereja Sundaresan, Cindy Wang, Ken X Wei, Christopher J Wood, Jeng-Bang Yau, Eric J Zhang, Oliver E Dial, Jerry M Chow, and Jay M Gambetta. “Demonstration of quantum volume 64 on a supercon-ducting quantum computing system”. *Quantum Sci. Technol.* **6**, 025020 (2021).
- [15] Yulin Wu, Wan-Su Bao, Sirui Cao, Fusheng Chen, Ming-Cheng Chen, Xiawei Chen, Tung-Hsun Chung, Hui Deng, Yajie Du, Daojin Fan, Ming Gong, Cheng Guo, Chu Guo, Shaojun Guo, Lianchen Han, Linyin Hong, He-Liang Huang, Yong-Heng Huo, Liping Li, Na Li, Shaowei Li, Yuan Li, Futian Liang, Chun Lin, Jin Lin, Hao-ran Qian, Dan Qiao, Hao Rong, Hong Su, Lihua Sun, Liangyuan Wang, Shiyu Wang, Dachao Wu, Yu Xu, Kai Yan, Weifeng Yang, Yang Yang, Yangsen Ye, Jiang-han Yin, Chong Ying, Jiale Yu, Chen Zha, Cha Zhang, Haibin Zhang, Kaili Zhang, Yiming Zhang, Han Zhao, Youwei Zhao, Liang Zhou, Qingling Zhu, Chao-Yang Lu, Cheng-Zhi Peng, Xiaobo Zhu, and Jian-Wei Pan. “Strong quantum computational advantage using a super-conducting quantum processor”. *Phys. Rev. Lett.* **127**, 180501 (2021).
- [16] W. Huang, C. H. Yang, K. W. Chan, T. Tanttu, B. Hensen, R. C. C. Leon, M. A. Fogarty, J. C. C. Hwang, F. E. Hudson, K. M. Itoh, A. Morello, A. Laucht, and A. S. Dzurak. “Fidelity benchmarks for two-qubit gates in silicon”. *Nature* **569**, 532–536 (2019).
- [17] S. A. Moses, C. H. Baldwin, M. S. Allman, R. An-cona, L. Ascarrunz, C. Barnes, J. Bartolotta, B. Bjork, P. Blanchard, M. Bohn, J. G. Bohnet, N. C. Brown, N. Q. Burdick, W. C. Burton, S. L. Campbell, J. P. Campora, C. Carron, J. Chambers, J. W. Chan, Y. H. Chen, A. Chernoguzov, E. Chertkov, J. Colina, J. P. Curtis, R. Daniel, M. DeCross, D. Deen, C. Delaney, J. M. Dreiling, C. T. Ertsgaard, J. Esposito, B. Estey, M. Fabrikant, C. Figgatt, C. Foltz, M. Foss-Feig, D. Franco, J. P. Gaebler, T. M. Gatterman, C. N. Gilbreth, J. Giles, E. Glynn, A. Hall, A. M. Hankin, A. Hansen, D. Hayes, B. Higashi, I. M. Hoffman, B. Horning, J. J. Hout, R. Jacobs, J. Johansen, L. Jones, J. Karcz, T. Klein, P. Lauria, P. Lee, D. Liefer, C. Lytle, S. T. Lu, D. Lucchetti, A. Malm, M. Matheny, B. Mathew-son, K. Mayer, D. B. Miller, M. Mills, B. Neyenhuis, L. Nugent, S. Olson, J. Parks, G. N. Price, Z. Price, M. Pugh, A. Ransford, A. P. Reed, C. Roman, M. Rowe, C. Ryan-Anderson, S. Sanders, J. Sedlacek, P. Shevchuk, P. Siegfried, T. Skripka, B. Spaun, R. T. Sprenkle, R. P. Stutz, M. Swallows, R. I. Tobey, A. Tran, T. Tran, E. Vogt, C. Volin, J. Walker, A. M. Zolot, and J. M. Pino. “A Race Track Trapped-Ion Quantum Processor” (2023). arXiv:2305.03828.
- [18] Daniel Gottesman. “Quantum fault tolerance in small experiments” (2016). arXiv:1610.03507.
- [19] Alexandre M. Souza, Jingfu Zhang, Colm A. Ryan, and Raymond Laflamme. “Experimental magic state distilla-tion for fault-tolerant quantum computing”. *Nat. Com-mun.* **2**, 169 (2011).
- [20] Jingfu Zhang, Raymond Laflamme, and Dieter Suter. “Experimental implementation of encoded logical qubit operations in a perfect quantum error correcting code”. *Phys. Rev. Lett.* **109**, 100503 (2012).
- [21] Daniel Nigg, Markus Mueller, Esteban A. Martinez, Philipp Schindler, Markus Hennrich, Thomas Monz, Miguel A. Martin-Delgado, and Rainer Blatt. “Ex-perimental Quantum Computations on a Topologi-cally Encoded Qubit”. *Science* **345**, 302–305 (2014). arxiv:1403.5426.
- [22] Laird Egan, Dripto M. Debroy, Crystal Noel, An-drew Risinger, Daiwei Zhu, Debopriyo Biswas, Michael Newman, Muyuan Li, Kenneth R. Brown, Marko Cetina, and Christopher Monroe. “Fault-Tolerant Op-eration of a Quantum Error-Correction Code” (2021). arxiv:2009.11482.
- [23] Lukas Postler, Sascha Heußen, Ivan Pogorelov, Manuel

- Rispler, Thomas Feldker, Michael Meth, Christian D. Marciniak, Roman Stricker, Martin Ringbauer, Rainer Blatt, Philipp Schindler, Markus Müller, and Thomas Monz. “Demonstration of fault-tolerant universal quantum gate operations”. *Nature* **605**, 675–680 (2022).
- [24] C. Ryan-Anderson, N. C. Brown, M. S. Allman, B. Arkin, G. Asa-Attuah, C. Baldwin, J. Berg, J. G. Bohnet, S. Braxton, N. Burdick, J. P. Campora, A. Chernoguzov, J. Esposito, B. Evans, D. Francois, J. P. Gaebler, T. M. Gatterman, J. Gerber, K. Gilmore, D. Gresh, A. Hall, A. Hankin, J. Hostetter, D. Lucchetti, K. Mayer, J. Myers, B. Neyenhuis, J. Santiago, J. Sedlacek, T. Skripka, A. Slattery, R. P. Stutz, J. Tait, R. Tobey, G. Vittorini, J. Walker, and D. Hayes. “Implementing Fault-tolerant Entangling Gates on the Five-qubit Code and the Color Code” (2022). [arXiv:2208.01863](https://arxiv.org/abs/2208.01863).
- [25] Christophe Vuillot. “Is error detection helpful on IBM 5Q chips?”. *Quantum Inf. Comput.* **18**, 0949–0964 (2018).
- [26] Robin Harper and Steven T. Flammia. “Fault-Tolerant Logical Gates in the IBM Quantum Experience”. *Phys. Rev. Lett.* **122**, 080504 (2019).
- [27] Riddhi S. Gupta, Neereja Sundaresan, Thomas Alexander, Christopher J. Wood, Seth T. Merkel, Michael B. Healy, Marius Hillenbrand, Tomas Jochym-O’Connor, James R. Wootton, Theodore J. Yoder, Andrew W. Cross, Maika Takita, and Benjamin J. Brown. “Encoding a magic state with beyond break-even fidelity” (2023). [arXiv:2305.13581](https://arxiv.org/abs/2305.13581).
- [28] Vlatko Vedral, Adriano Barenco, and Artur Ekert. “Quantum networks for elementary arithmetic operations”. *Phys. Rev. A* **54**, 147–153 (1996).
- [29] Craig Gidney. “Halving the cost of quantum addition”. *Quantum* **2**, 74 (2018).
- [30] Peter W. Shor. “Polynomial-Time Algorithms for Prime Factorization and Discrete Logarithms on a Quantum Computer”. *SIAM J. Comput.* **26**, 1484–1509 (1997).
- [31] Craig Gidney and Martin Ekerå. “How to factor 2048 bit RSA integers in 8 hours using 20 million noisy qubits”. *Quantum* **5**, 433 (2021).
- [32] Daniel Gottesman. “Stabilizer Codes and Quantum Error Correction”. PhD thesis. Caltech. (1997). [arxiv:quant-ph/9705052](https://arxiv.org/abs/quant-ph/9705052).
- [33] A. R. Calderbank and Peter W. Shor. “Good quantum error-correcting codes exist”. *Phys. Rev. A* **54**, 1098–1105 (1996).
- [34] A. M. Steane. “Multiple-particle interference and quantum error correction”. *Proc. R. Soc. Lond. A* **452**, 2551–2577 (1996).
- [35] Michael A. Nielsen and Isaac L. Chuang. “Quantum computation and quantum information: 10th anniversary edition”. Cambridge University Press. (2010).
- [36] Rui Chao and Ben W. Reichardt. “Quantum error correction with only two extra qubits”. *Phys. Rev. Lett.* **121**, 050502 (2018).
- [37] “IBM Quantum”. <https://quantum-computing.ibm.com/>.
- [38] Jared B. Hertzberg, Eric J. Zhang, Sami Rosenblatt, Easwar Magesan, John A. Smolin, Jeng-Bang Yau, Vivekananda P. Adiga, Martin Sandberg, Markus Brink, Jerry M. Chow, and Jason S. Orcutt. “Laser-annealing Josephson junctions for yielding scaled-up superconducting quantum processors”. *npj Quantum Inf.* **7**, 129 (2021).
- [39] “Getting started with Native Gates”. <https://ionq.com/docs/getting-started-with-native-gates>.
- [40] Earl T. Campbell and Mark Howard. “Unifying gate synthesis and magic state distillation”. *Phys. Rev. Lett.* **118**, 060501 (2017).
- [41] Earl T. Campbell and Mark Howard. “Unified framework for magic state distillation and multiqubit gate synthesis with reduced resource cost”. *Phys. Rev. A* **95**, 022316 (2017).
- [42] Jeongwan Haah and Matthew B. Hastings. “Codes and Protocols for Distilling T , controlled- S , and Toffoli Gates”. *Quantum* **2**, 71 (2018).
- [43] Sepehr Nezami and Jeongwan Haah. “Classification of small triorthogonal codes”. *Phys. Rev. A* **106**, 012437 (2022).
- [44] Jingzhen Hu, Qingzhong Liang, and Robert Calderbank. “Designing the Quantum Channels Induced by Diagonal Gates”. *Quantum* **6**, 802 (2022).
- [45] Mark A. Webster, Armanda O. Quintavalle, and Stephen D. Bartlett. “Transversal Diagonal Logical Operators for Stabiliser Codes” (2023). [arXiv:2303.15615](https://arxiv.org/abs/2303.15615).
- [46] Markus Grassl and Martin Roetteler. “Leveraging automorphisms of quantum codes for fault-tolerant quantum computation”. In 2013 IEEE International Symposium on Information Theory. Pages 534–538. (2013).
- [47] Rui Chao and Ben W. Reichardt. “Fault-tolerant quantum computation with few qubits”. *npj Quantum Inf.* **4**, 42 (2018).
- [48] Yang Wang, Selwyn Simsek, and Ben Criger. “Fault-tolerant one-bit addition with the smallest interesting colour code”. To appear (2023).

Appendix A: Additional experimental details

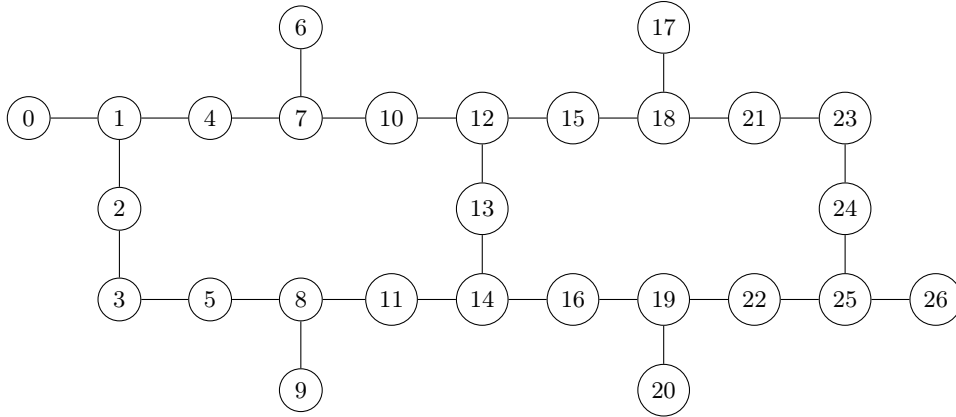


Figure 6. Layout of the `ibmq_mumbai` device. Vertices represent qubits and edges represent the availability of entangling gates between the two endpoints. The mapping from the qubits of the $[[8,3,2]]$ code to the qubits of the device was $(q_0, 7)$, $(q_1, 4)$, $(q_2, 1)$, $(q_3, 10)$, $(q_4, 2)$, $(q_5, 10)$, $(q_6, 13)$, $(q_7, 3)$.

Appendix B: Additional experimental results

1. Logical Z basis measurement results

For the experiments with $|+++ \rangle$ state preparation and Z basis measurement, we observe improved performance for the encoded circuits containing a transversal non-Clifford gate; see Fig. 7. And for the experiments with $|GHZ \rangle$ state preparation and Z basis measurement, we observe improved performance for all of the encoded circuits; see Fig. 8. We note that in these cases the gates have no effect on the expected output measurement distribution, as the gates commute with the measurements.

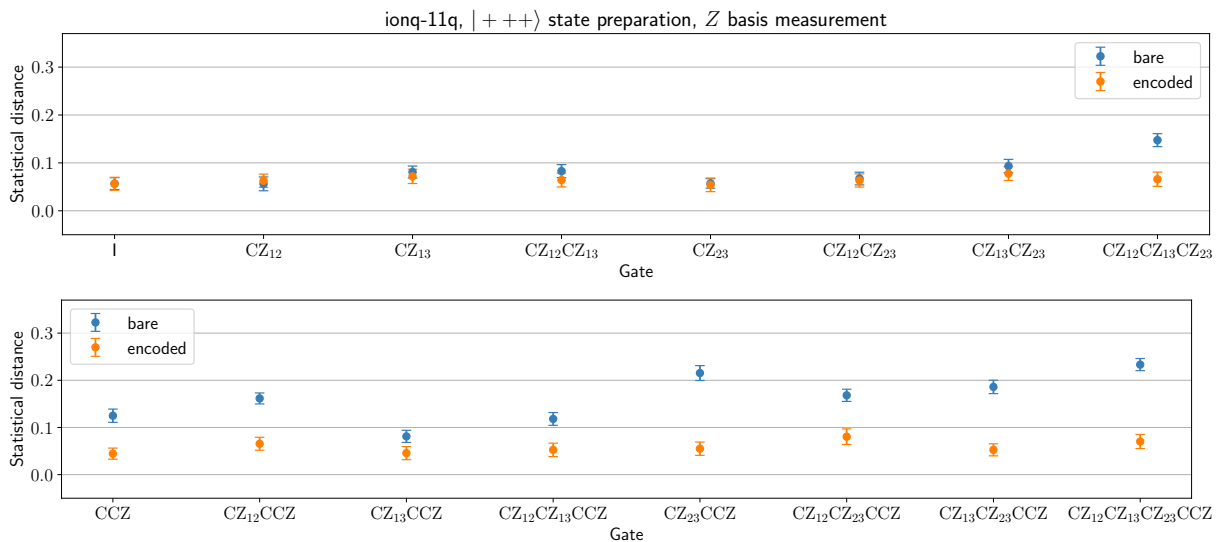


Figure 7. Performance of bare (unencoded) and encoded versions of circuits for preparing states of the form $g|+++ \rangle$, where g is a transversal gate of the $[[8,3,2]]$ code. In each case, we measure the qubits in the Z basis and we plot the statistical distance of the observed measurement distribution from the ideal distribution. Each data point represents 1024 shots of the circuit performed on `ionq-11q`, and we use bootstrap resampling to calculate the error bars.

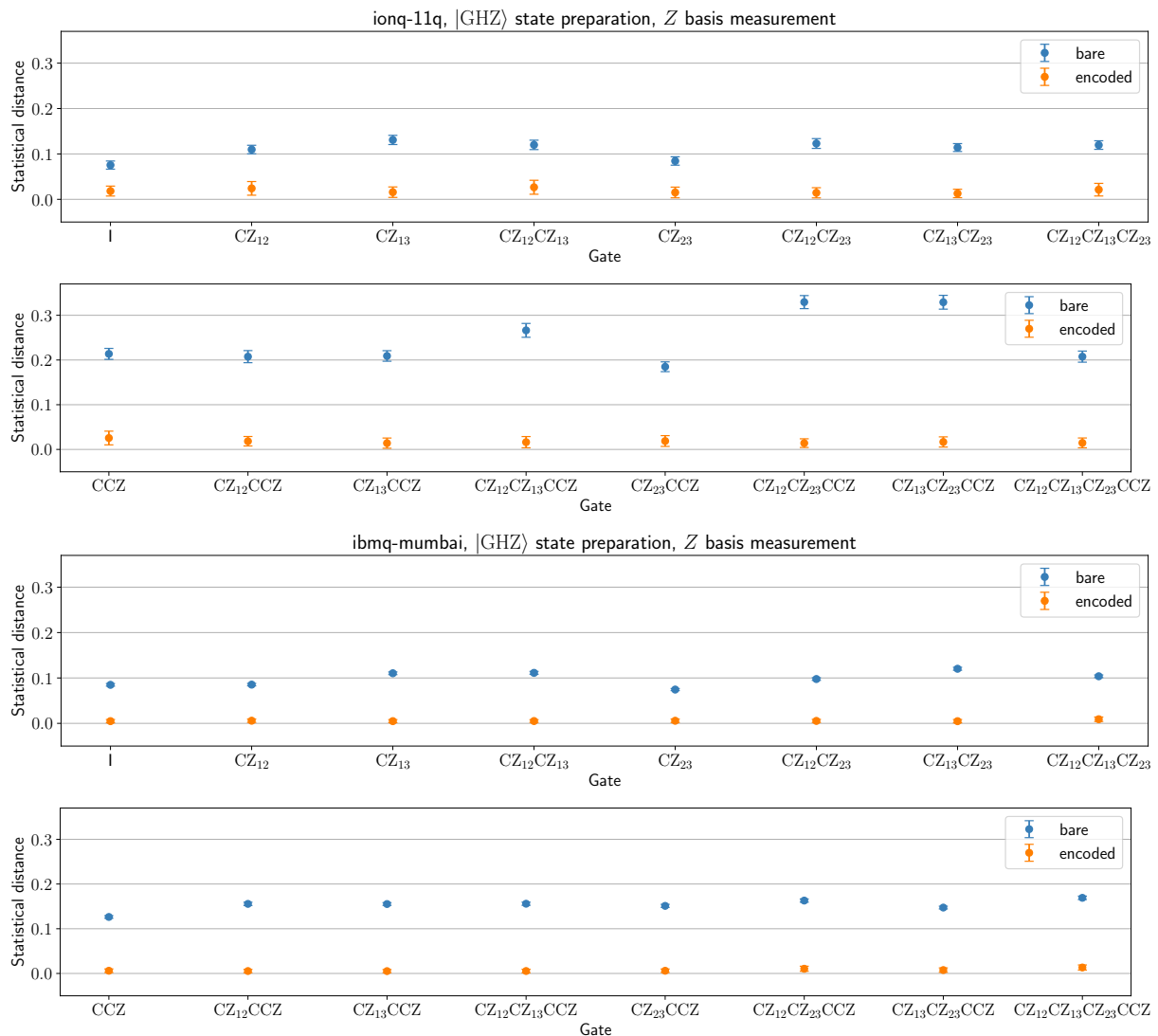


Figure 8. Performance of bare (unencoded) and encoded versions of circuits for preparing states of the form $g|\text{GHZ}\rangle$, where g is a transversal gate of the $[[8,3,2]]$ code. In each case, we measure the qubits in the Z basis and we plot the statistical distance of the observed measurement distribution from the ideal distribution. The upper two plots show the data for `ionq-11q`, where we ran 1024 shots for each circuit, and the lower two plots show the data for `ibmq-mumbai` where we ran 10,000 shots for each circuit. In both cases, the error bars are calculated using bootstrap resampling.

2. Post-selection rates

In this appendix, we provide the post-selection rates (proportion of accepted shots) for our experiments. Two-qubit gates and measurements are the noisiest operations in superconducting and trapped-ion devices [13, 14], hence we can approximate the error model in these devices with ideal state preparation and one-qubit gates, but noisy two-qubit gates and measurements (1% error rate). Suppose that any two-qubit gate error or measurement error causes us to discard the run, then (to first order) we would expect a post-selection rate of $1 - 0.01(n_m + n_g)$, where n_m is the number of measurements and n_g is the number of two-qubit gates. By counting the relevant locations in Figs. 2 and 3, we therefore estimate a post-selection rate of 69% and 86% for the circuits with $|+++ \rangle$ and $|\text{GHZ}\rangle$ state preparation, respectively. These estimates are reasonably close to the values we observe in our experiments; see Tables I to III.

State	Gate	Measurement	Device	Post-selection rate
$ +++ \rangle$	I	X basis	ionq-11q	78%
$ +++ \rangle$	CZ_{12}	X basis	ionq-11q	78%
$ +++ \rangle$	CZ_{13}	X basis	ionq-11q	69%
$ +++ \rangle$	$CZ_{12}CZ_{13}$	X basis	ionq-11q	76%
$ +++ \rangle$	CZ_{23}	X basis	ionq-11q	80%
$ +++ \rangle$	$CZ_{12}CZ_{23}$	X basis	ionq-11q	77%
$ +++ \rangle$	$CZ_{13}CZ_{23}$	X basis	ionq-11q	79%
$ +++ \rangle$	$CZ_{12}CZ_{13}CZ_{23}$	X basis	ionq-11q	80%
$ +++ \rangle$	CCZ	X basis	ionq-11q	75%
$ +++ \rangle$	$CZ_{12}CCZ$	X basis	ionq-11q	81%
$ +++ \rangle$	$CZ_{13}CCZ$	X basis	ionq-11q	74%
$ +++ \rangle$	$CZ_{12}CZ_{13}CCZ$	X basis	ionq-11q	84%
$ +++ \rangle$	$CZ_{23}CCZ$	X basis	ionq-11q	75%
$ +++ \rangle$	$CZ_{12}CZ_{23}CCZ$	X basis	ionq-11q	83%
$ +++ \rangle$	$CZ_{13}CZ_{23}CCZ$	X basis	ionq-11q	77%
$ +++ \rangle$	$CZ_{12}CZ_{13}CZ_{23}CCZ$	X basis	ionq-11q	77%
$ +++ \rangle$	I	Z basis	ionq-11q	73%
$ +++ \rangle$	CZ_{12}	Z basis	ionq-11q	78%
$ +++ \rangle$	CZ_{13}	Z basis	ionq-11q	71%
$ +++ \rangle$	$CZ_{12}CZ_{13}$	Z basis	ionq-11q	74%
$ +++ \rangle$	CZ_{23}	Z basis	ionq-11q	72%
$ +++ \rangle$	$CZ_{12}CZ_{23}$	Z basis	ionq-11q	72%
$ +++ \rangle$	$CZ_{13}CZ_{23}$	Z basis	ionq-11q	73%
$ +++ \rangle$	$CZ_{12}CZ_{13}CZ_{23}$	Z basis	ionq-11q	71%
$ +++ \rangle$	CCZ	Z basis	ionq-11q	74%
$ +++ \rangle$	$CZ_{12}CCZ$	Z basis	ionq-11q	74%
$ +++ \rangle$	$CZ_{13}CCZ$	Z basis	ionq-11q	70%
$ +++ \rangle$	$CZ_{12}CZ_{13}CCZ$	Z basis	ionq-11q	74%
$ +++ \rangle$	$CZ_{23}CCZ$	Z basis	ionq-11q	72%
$ +++ \rangle$	$CZ_{12}CZ_{23}CCZ$	Z basis	ionq-11q	73%
$ +++ \rangle$	$CZ_{13}CZ_{23}CCZ$	Z basis	ionq-11q	74%
$ +++ \rangle$	$CZ_{12}CZ_{13}CZ_{23}CCZ$	Z basis	ionq-11q	73%

Table I. Post-selection rates for the results shown in Figs. 5 and 7, where the percentage indicates the proportion of shots that were accepted. The average post-selection rate was 75%.

State	Gate	Measurement	Device	Post-selection rate
$ \text{GHZ}\rangle$	I	X basis	ionq-11q	90%
$ \text{GHZ}\rangle$	CZ_{12}	X basis	ionq-11q	86%
$ \text{GHZ}\rangle$	CZ_{13}	X basis	ionq-11q	90%
$ \text{GHZ}\rangle$	$CZ_{12}CZ_{13}$	X basis	ionq-11q	78%
$ \text{GHZ}\rangle$	CZ_{23}	X basis	ionq-11q	83%
$ \text{GHZ}\rangle$	$CZ_{12}CZ_{23}$	X basis	ionq-11q	81%
$ \text{GHZ}\rangle$	$CZ_{13}CZ_{23}$	X basis	ionq-11q	82%
$ \text{GHZ}\rangle$	$CZ_{12}CZ_{13}CZ_{23}$	X basis	ionq-11q	79%
$ \text{GHZ}\rangle$	CCZ	X basis	ionq-11q	80%
$ \text{GHZ}\rangle$	$CZ_{12}CCZ$	X basis	ionq-11q	78%
$ \text{GHZ}\rangle$	$CZ_{13}CCZ$	X basis	ionq-11q	82%
$ \text{GHZ}\rangle$	$CZ_{12}CZ_{13}CCZ$	X basis	ionq-11q	87%
$ \text{GHZ}\rangle$	$CZ_{23}CCZ$	X basis	ionq-11q	83%
$ \text{GHZ}\rangle$	$CZ_{12}CZ_{23}CCZ$	X basis	ionq-11q	83%
$ \text{GHZ}\rangle$	$CZ_{13}CZ_{23}CCZ$	X basis	ionq-11q	82%
$ \text{GHZ}\rangle$	$CZ_{12}CZ_{13}CZ_{23}CCZ$	X basis	ionq-11q	84%
$ \text{GHZ}\rangle$	I	Z basis	ionq-11q	86%
$ \text{GHZ}\rangle$	CZ_{12}	Z basis	ionq-11q	81%
$ \text{GHZ}\rangle$	CZ_{13}	Z basis	ionq-11q	84%
$ \text{GHZ}\rangle$	$CZ_{12}CZ_{13}$	Z basis	ionq-11q	85%
$ \text{GHZ}\rangle$	CZ_{23}	Z basis	ionq-11q	81%
$ \text{GHZ}\rangle$	$CZ_{12}CZ_{23}$	Z basis	ionq-11q	90%
$ \text{GHZ}\rangle$	$CZ_{13}CZ_{23}$	Z basis	ionq-11q	84%
$ \text{GHZ}\rangle$	$CZ_{12}CZ_{13}CZ_{23}$	Z basis	ionq-11q	81%
$ \text{GHZ}\rangle$	CCZ	Z basis	ionq-11q	86%
$ \text{GHZ}\rangle$	$CZ_{12}CCZ$	Z basis	ionq-11q	80%
$ \text{GHZ}\rangle$	$CZ_{13}CCZ$	Z basis	ionq-11q	87%
$ \text{GHZ}\rangle$	$CZ_{12}CZ_{13}CCZ$	Z basis	ionq-11q	75%
$ \text{GHZ}\rangle$	$CZ_{23}CCZ$	Z basis	ionq-11q	74%
$ \text{GHZ}\rangle$	$CZ_{12}CZ_{23}CCZ$	Z basis	ionq-11q	83%
$ \text{GHZ}\rangle$	$CZ_{13}CZ_{23}CCZ$	Z basis	ionq-11q	75%
$ \text{GHZ}\rangle$	$CZ_{12}CZ_{13}CZ_{23}CCZ$	Z basis	ionq-11q	85%

Table II. Post-selection rates for the results shown in Figs. 4 and 8 for the IonQ device, where the percentage indicates the proportion of shots that were accepted. The average post-selection rate was 83%.

State	Gate	Measurement	Device	Post-selection rate
$ \text{GHZ}\rangle$	I	X basis	ibmq_mumbai	76%
$ \text{GHZ}\rangle$	CZ_{12}	X basis	ibmq_mumbai	69%
$ \text{GHZ}\rangle$	CZ_{13}	X basis	ibmq_mumbai	72%
$ \text{GHZ}\rangle$	$CZ_{12}CZ_{13}$	X basis	ibmq_mumbai	79%
$ \text{GHZ}\rangle$	CZ_{23}	X basis	ibmq_mumbai	69%
$ \text{GHZ}\rangle$	$CZ_{12}CZ_{23}$	X basis	ibmq_mumbai	76%
$ \text{GHZ}\rangle$	$CZ_{13}CZ_{23}$	X basis	ibmq_mumbai	78%
$ \text{GHZ}\rangle$	$CZ_{12}CZ_{13}CZ_{23}$	X basis	ibmq_mumbai	80%
$ \text{GHZ}\rangle$	CCZ	X basis	ibmq_mumbai	72%
$ \text{GHZ}\rangle$	$CZ_{12}CCZ$	X basis	ibmq_mumbai	73%
$ \text{GHZ}\rangle$	$CZ_{13}CCZ$	X basis	ibmq_mumbai	79%
$ \text{GHZ}\rangle$	$CZ_{12}CZ_{13}CCZ$	X basis	ibmq_mumbai	76%
$ \text{GHZ}\rangle$	$CZ_{23}CCZ$	X basis	ibmq_mumbai	73%
$ \text{GHZ}\rangle$	$CZ_{12}CZ_{23}CCZ$	X basis	ibmq_mumbai	79%
$ \text{GHZ}\rangle$	$CZ_{13}CZ_{23}CCZ$	X basis	ibmq_mumbai	79%
$ \text{GHZ}\rangle$	$CZ_{12}CZ_{13}CZ_{23}CCZ$	X basis	ibmq_mumbai	72%
$ \text{GHZ}\rangle$	I	Z basis	ibmq_mumbai	74%
$ \text{GHZ}\rangle$	CZ_{12}	Z basis	ibmq_mumbai	70%
$ \text{GHZ}\rangle$	CZ_{13}	Z basis	ibmq_mumbai	74%
$ \text{GHZ}\rangle$	$CZ_{12}CZ_{13}$	Z basis	ibmq_mumbai	77%
$ \text{GHZ}\rangle$	CZ_{23}	Z basis	ibmq_mumbai	71%
$ \text{GHZ}\rangle$	$CZ_{12}CZ_{23}$	Z basis	ibmq_mumbai	71%
$ \text{GHZ}\rangle$	$CZ_{13}CZ_{23}$	Z basis	ibmq_mumbai	75%
$ \text{GHZ}\rangle$	$CZ_{12}CZ_{13}CZ_{23}$	Z basis	ibmq_mumbai	73%
$ \text{GHZ}\rangle$	CCZ	Z basis	ibmq_mumbai	76%
$ \text{GHZ}\rangle$	$CZ_{12}CCZ$	Z basis	ibmq_mumbai	78%
$ \text{GHZ}\rangle$	$CZ_{13}CCZ$	Z basis	ibmq_mumbai	78%
$ \text{GHZ}\rangle$	$CZ_{12}CZ_{13}CCZ$	Z basis	ibmq_mumbai	77%
$ \text{GHZ}\rangle$	$CZ_{23}CCZ$	Z basis	ibmq_mumbai	78%
$ \text{GHZ}\rangle$	$CZ_{12}CZ_{23}CCZ$	Z basis	ibmq_mumbai	77%
$ \text{GHZ}\rangle$	$CZ_{13}CZ_{23}CCZ$	Z basis	ibmq_mumbai	77%
$ \text{GHZ}\rangle$	$CZ_{12}CZ_{13}CZ_{23}CCZ$	Z basis	ibmq_mumbai	71%

Table III. Post-selection rates for the results shown in Figs. 4 and 8 for the IBM device, where the percentage indicates the proportion of shots that were accepted. The average post-selection rate was 75%.